The attraction between like-charged macroions—the crucial roles of macroion geometry and charge distribution

2004 J. Phys.: Condens. Matter 16 2907

(http://iopscience.iop.org/0953-8984/16/16/015)

INSTITUTE OF PHYSICS PUBLISHING JOURNAL OF PHYSICS: CONDENSED MATTER

J. Phys.: Condens. Matter **16** (2004) 2907–2930 PII: S0953-8984(04)72768-X

The attraction between like-charged macroions—the crucial roles of macroion geometry and charge distribution

Arup K Mukherjee

Department of Physics, University of Puerto Rico, Box 23343 UPR Station, San Juan, PR 00931-3343, USA

Received 25 November 2003
Published 8 April 2004
Online at stacks.iop.org/JPhysCM/16/2907
DOI: 10.1088/0953-8984/16/16/015

Abstract

A mechanism of attraction between like-charged macroions due to charge fluctuation has been revisited for macroions of different geometries. For higher charge asymmetry, macroion geometry plays an important role in charge fluctuation, while for comparatively lower charge asymmetry the fluctuation is almost independent of the geometry. At very low temperatures and in a high Coulomb coupling regime, stable ionized states due to auto-ionization are able to exist, which leads to long range Coulomb attraction. Overcharging of a single macroion and its counterion distribution minimizing the total energy has been studied briefly to explain the attraction properties between two like-charged macroions. The investigations have been carried out using a technique based on total energy minimization which has been verified successfully for some special cases with molecular dynamics simulation results previously published. A theoretical model, derived by modifying the Scatchard approach, is proposed to explain the overcharging curves obtained from the simulation. It has been found that the model is equally efficient for both spherical and non-spherical macroion geometries. Wigner crystal theory has also been employed for spherical cases, and excellent agreement has been found between the two theoretical approaches.

1. Introduction

The attraction between two like-charged macroions, one of the most interesting counter-intuitive phenomena, can originate from a number of mechanisms [1, 2]. Auto-ionization is one of them, which has recently been studied extensively [3–5] for spherical macroions. Auto-ionization originates from mutual counterion transfer between a pair of macroions, leading to one macroion being overcharged and the other undercharged. Due to overcharging, the effective charge of the macroion becomes opposite to its bare charge and also to the effective

charge of the other (undercharged) macroion. Overcharging or overscreening [3–7] stems from ionic correlation [7–11] which cannot be explained using mean field theories [12–15] because such theories ignore ionic correlation.

To understand how auto-ionization leads to strong long range attraction between charged macroions, one needs to focus on the overcharging phenomenon of a single macroion. Overcharging a spherical macroion at $T = 0$ resembles the classic Thomson problem of finding the ground state of charges confined to a sphere. This has recently attracted huge attention because of its possible application to colloidal and polyelectrolyte solutions and particularly to biological systems containing multivalent counterions. The Thomson problem is a 100 year old puzzle originating from the classical work of Thomson [16]. A large number of papers have already been published [17–39] (listed chronologically) attacking it in various analytical approaches. Since the principal goal of this paper is to focus on the influence of the macroion geometry on the attraction mechanism between a pair of macroions, the discussion of the Thomson problem is not considered here, and the relevant overcharging phenomenon will be expressed in terms of the above-stated ionic correlations only.

When a macroion (initially neutralized by counterions) is being overcharged, ionic correlation builds up between the counterions on the surface of the macroion, which causes a gradual decrease in total electrostatic energy with adsorption of counterions up to a certain number. The maximum number of counterions adsorbed by the macroion ('maximal acceptance'), which corresponds to the lowest electrostatic energy of the macroion complex (macroion and counterions condensed on macroion surface) depends on the macroion bare charge. This number has been seen to increase with the increase of the macroion bare charge. Similarly, the strength of attraction between a pair of undercharged and overcharged macroions increases with the increase in difference of their bare charges, since the macroion bare charge asymmetry is directly related to the difference in correlation energies of the macroions [3]. In this study, it is shown that if the macroion charge asymmetry is high enough, a 'stable' ionized ground state is possible to exist, and the energy variation due to ionization is nearly independent of the macroion geometry and size for lower macroion charge asymmetry, while for higher charge asymmetry, it does depend on both the macroion geometry and size.

In the following, a technique based on electrostatic energy minimization will be elaborated and later employed. Next, the properties of overcharging of a single macroion with different geometries and sizes will be considered. In addition, the attraction phenomena due to auto-ionization between a pair of macroions with different geometries and sizes will be discussed in detail. For both a single macroion and a pair of macroions, two analytical models will be discussed and verified by the simulation results.

2. The energy minimization technique

In this paper, an intuitively simple technique based on the minimization of electrostatic energy has been employed to study the phenomenon of charge inversion. Usually energy minimization (EM) is an inherent phenomenon in a bound system. In any force field, whenever a bound system forms, it tries to minimize its configurational energy for stability, which is the basic idea behind this technique. Since the potential energy is a function only of distance, the members of the system arrange themselves to achieve a minimum energy configuration generally by maximizing their mutual distances. The electrostatic interaction energy between a spherical macroion of charge $+Q$ and radius R and a given number of point-like counterions of charge $-q_i$ each is proportional to $-\frac{Q\sum_i q_i}{R} + \sum_{i<j} \frac{q_i q_j}{r_{ij}}$, where r_{ij} is the direct distance between any two counterions i and j. Here r_{ij} is the only variable parameter depending on which energy is determined. In this case the bigger the r_{ij} the smaller the energy. Thus, to minimize the energy,

r_{ij} needs to be maximized. Note that in both Monte Carlo (MC) and molecular dynamics (MD) simulations, some type of energy minimization, subject to some given criteria, is effected.

The above approach has been extended to two other non-spherical geometries, an oblate spheroid and a spherocylinder, to investigate the pattern of the charge inversion and ion distribution in non-spherical geometries. It will be further discussed and shown that the degree of charge inversion is influenced by the macroion geometries. One of the reasons behind the choice of these geometries is that the oblate spheroid and spherocylinder can be imagined to be deformed shapes of a sphere as though a sphere were pressed (oblate spheroid) or pulled (spherocylinder) from two opposite sides. By deforming the spherical macroion gradually, one can clearly see the change in electrostatic energy of interaction between the macroion and surrounding counterions on its surface. Another reason is that many biological organisms and chemical macromolecules have shapes very similar to an oblate spheroid (namely globular proteins) and spherocylinder (namely tobacco mosaic virus, double helix DNA, F-actin, microtubules [44]). Thus, the aim of this study is three fold:

(i) to propose a simple technique, and
(ii) to investigate the effect of macroion geometry and/or macroion charge distribution on the overall charge inversion and counterion distribution, and
(iii) to examine the influence of macroion geometry and charge asymmetry on the inter-macroion attraction due to auto-ionization.

Since the ground state energy configuration ($T = 0$) is considered, the provisions on ion move acceptance of the Metropolis algorithm of a traditional MC simulation cannot be applied completely in this study. Moreover, only one final configuration is required for this system: that which has the lowest possible total electrostatic potential energy. In this technique, that final configuration has been achieved via following three steps. First, the neutral state is considered, where the total counterion charge is equal to the bare charge of the macroion. The average distance between the counterions is then estimated as $d \cong 2\sqrt{\frac{4\pi R^2}{\pi N_c}}$, where $4\pi R^2$ is the surface area of the macroion and N_c is the number of counterions. Since the surface areas of non-spherical macroions are the same as those of the spherical ones, this estimation of average inter-ionic distance is also valid for spherocylinders and oblate spheroids. The counterion positions are generated randomly on the surface of the macroion, keeping an initial inter-ionic distance of at least 40% of the estimated d. Note that, if $0.4d$ is less than the diameter of a counterion, one needs to consider a bigger initial inter-ionic distance to avoid the possibility of overlapping. If the position of any ion is less than $0.4d$ from any of its neighbour, the coordinates of that ion are regenerated repeatedly (up to a certain maximum number, typically not more than 10 000 times) until it maintains the required distance. The choice of initial inter-ionic distance also depends on τ. In the case of non-spherical geometries, for example a spherocylinder, the counterions may not occupy the whole surface area of the macroion. To minimize the electrostatic energy, most of the counterions generally accumulate on the cylindrical area of the spherocylinder. This is why it is necessary to consider an initial distance much lower than the average inter-ionic distance, especially in case of non-spherical geometry. When all the counterions are positioned on the macroion surface the total electrostatic energy (N_c counterions and macroion) is measured. The inter-ionic distance is gradually increased from its initial value (in this study, 500 steps have been considered) and after each increase the above procedure is followed a number of times (10 000 in this study) to achieve a lower energy configuration. The process can continue until the inter-ionic distance reaches at least $0.95d$. In this way the whole process generates a huge number of counterion configurations ($500 \times 10\,000$). Among all these configurations, only the lowest energy configuration is

accepted. The ion coordinates of this configuration are then transferred to the second steps where any of these counterions can move up to a maximum distance $d/2$ about its position for further energy minimization. In this step an ion is chosen at random and is moved randomly on the macroion surface. After each movement of any ion, the total electrostatic energy of the whole system is calculated. The move is accepted only if it causes a decrease in total energy. Note that, in this technique, the total energy is only allowed to decrease (contrary to the usual MC concept) and finally reaches the lowest energy configuration. In all cases, each ion attempts approximately one million moves (iteration) before the final configuration of the system is reached. In the third step (overcharging), starting from the neutral state, one counterion at a time is added to the system, and following the above two steps the lowest possible energy configuration is found for each addition.

The displacement parameter (DP) or step length is defined as the extent of maximum movement of an ion which adjusts itself (in a random manner) until an ion move is accepted. Varying the DP is the most essential part of this technique. The adjustment of the DP has been done in the following manner. At the very beginning of the second step of the simulation, an initial DP has been assigned which is approximately equal to the average distance between two adjacent ions (d). This value of the DP does not change until the acceptance continues, since a particular value of the DP can cause a decrease in energy by means of acceptance of ion movements towards a required direction and extent. The initial DP brings the system to its first local minimum energy state and no further decrease in energy is observed. When the decrease in energy stops (due to unaccepted ion moves) the DP is supposed to start changing its value randomly after each unaccepted ion move. But before changing its value (randomly), the last value of the DP is held fixed for a given number (generally 100 or less) of iterations (an iteration is defined as an attempt to move an ion, no matter whether it is accepted or not) for more acceptance. If any acceptance occurs within these 100 iterations, the DP does not change for the next 100 iterations. Had this trend continued, the DP would not change at all. If no acceptance occurs within these 100 iterations, the DP starts adjusting itself randomly until an ion move is accepted. Finally the DP finds a suitable new value (generally smaller than before) which initiates acceptance of each of the subsequent moves (or with an interval of a maximum 100 unaccepted moves) for a number of iterations, and the energy is seen to decrease until the system reaches the next state of local minimum energy (see figure 1). The above process is repeated a number of times until the system reaches very close to the true ground state. It has been seen that this short discontinuity in fluctuation of the DP is unavoidable and has a profound impact on quick energy minimization. Such fluctuations of the DP actually help to break the spatial counterion arrangements which cause the local minima, and help to reach a new minimum. Note that random adjustment of the DP is not required for the first step.

It is customary in traditional MC simulations to vary the displacement of a particle randomly within a slowly varying or fixed DP to achieve a predetermined acceptance percentage. Early statements clarify that the DP remains fixed in this technique when the system energy gradually decreases between two local minima (which implies nearly continuous acceptance). But when the system reaches a local minimum, the DP itself fluctuates randomly. Thus the ion fluctuations are intensified by double random effects. It has been observed that at a specific local minimum, the length of the DP can become momentarily bigger than the length it had just before reaching the minimum. This can cause strides of the ions over the macroion surface, which is very similar to a suddenly increased temperature state.

Normally, during the simulation run, the DP gradually decreases (except for some sudden increases near local minima) while the system passes through a series of such states of increasingly lower energies. It is seen (after a sufficient number of iterations) that even after the displacement parameter is adjusted to a value less than 10^{-6} Å, the energy continues

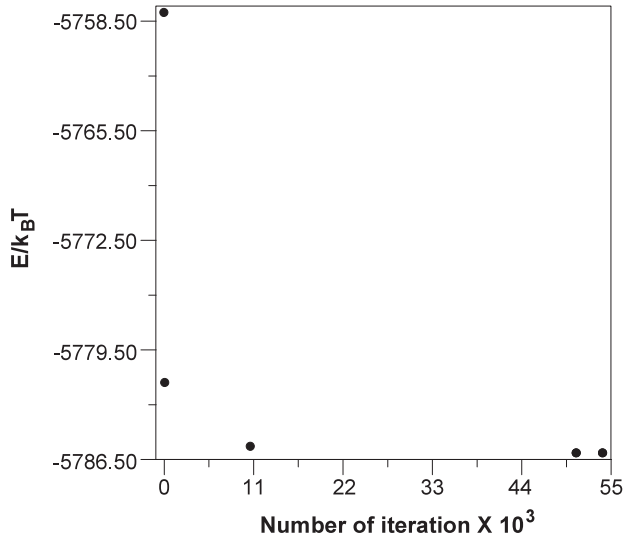

Figure 1. The change of displacement parameter (DP) and consequently the decrease in total energy of the macroion complex as the simulation proceeds. Each point (filled circle) indicates a state of local minimum energy and represents a change in DP which is automatically selected by the program depending on the acceptance of an ion movement.

decreasing, but the energy changes are infinitesimally small. In those cases it is assumed that the system is very close to the true ground state. It is extremely challenging to reach the true ground state since the nearly degenerate metastable states grow exponentially [32] (also see figure 1). Indeed, for the purposes of the present study, knowledge of the exact ground state energy is really not necessary since one wants only to be sufficiently close to the ground state energy.

3. Single macroion overcharging

3.1. Simulation model

The system considered in this study is comprised of an isolated macroion with bare charge $Q = -Z_{\mathrm{m}}|e|$ surrounded by a number N_{c} of small counterions with charge $q = Z_{\mathrm{c}}|e|$, so that $Q = -N_{\mathrm{c}}Z_{\mathrm{c}}|e|$ is the neutral state. Following Messina *et al* [3] the value $Z_{\mathrm{c}} = 2$ is chosen for all the calculations. All these counterions are always kept at a constant counterion–macroion distance of closest approach (hard core). The non-spherical macroions considered here are oblate spheroids and spherocylinders, as stated earlier. The spherocylinder is a cylinder of length L and radius r sandwiched between two hemispherical end caps of the same radius r (figure 2). Thus the length of the cylinder[1] is $L = r\tau$. In the oblate spheroid, the centres of curvature A and B of the two hemispherical sections a and b are at a distance L (figure 3) apart. Obviously, if $\tau = 0$, the two non-spherical geometries reduce to sphere. For all the geometries the surfaces have been kept same as that of a sphere of radius $R = 28.56$ Å since in Wigner

[1] The 'shape factor' τ is an important parameter in this study, as it governs the geometry (shape) and size of the macroions. With the change of size (length and width), the surface of an oblate spheroid or a spherocylinder is kept the same as that of a sphere of fixed radius R to maintain the same surface charge density. In case of a spherocylinder, when the length L of the cylinder is changed, the radius of the hemispherical end caps r_m is also changed to keep the same surface as shown in equation (A.2). The shape factor is defined as $\tau = L/r$; in terms of τ, the aspect ratio of the spherocylinder $= L/(2r) = \tau/2$.

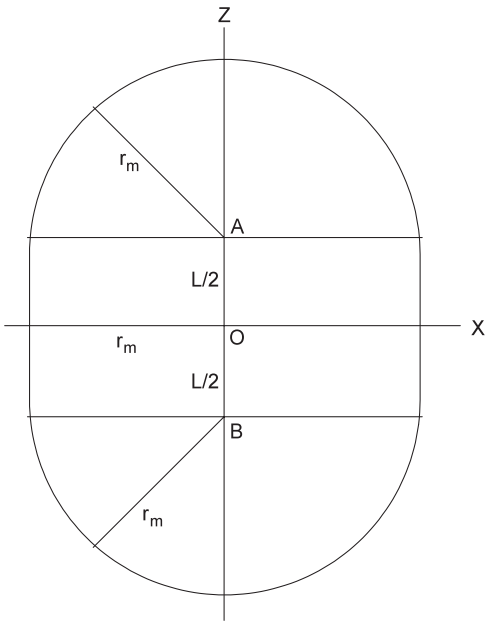

Figure 2. A spherocylinder. A and B are the centres of the two end caps which are distance L apart (L is also the length of the cylinder).

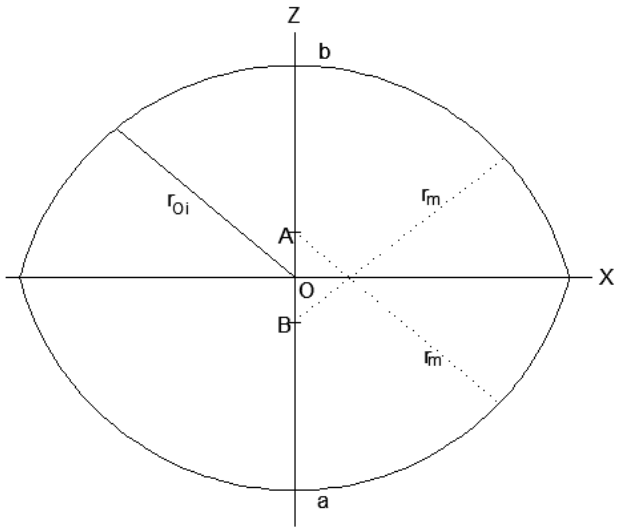

Figure 3. An oblate spheroid. A and B are the centres of curvature of the two equal sections a and b of a sphere of radius r_m. The centres A and B are at distance L apart. The point O is considered as the centre of the oblate spheroid.

crystal (WC) theory, the energy gains scale with the surface counterion concentration and thus this allows different geometries that are comparable in terms of WC theory.

The computer routine had been made in such a way that it could calculate minimum energy configurations for any of the three models used in this study by choosing only one of

the three following values of the 'shape factor': $\tau = 0$ (sphere), $\tau < 0$ (oblate spheroid), $\tau > 0$ (spherocylinder).

The internal charge distribution of a non-spherical macroion plays important roles in counterion distribution and energy minimization. Charge distribution will be discussed in section 3. As a plausible assumption, a single central point charge at O (figure 3) for an oblate spheroid and a line charge AB for a spherocylinder (figure 2) have been investigated in this study. Under these assumptions the Coulombic potential energies for the three geometries can be written straightforwardly.

3.1.1. Spherocylinder ($\tau > 0$).

$$E = \frac{|e|^2}{4\pi\varepsilon_0\varepsilon_r}\left[C_\lambda Z_c \sum_i \ln\left[\frac{1+\sin(\psi_{2i})}{1-\sin(\psi_{1i})}\frac{\cos(\psi_{1i})}{\cos(\psi_{2i})}\right] + \sum_{i<j}\frac{Z_c^2}{r_{ij}}\right] \tag{1}$$

where

$$\begin{aligned} C_\lambda &= Z_m/L \\ \psi_{1i} &= \tan^{-1}\left[\frac{(L/2-z_i)}{r_m\cos\theta_i}\right] \\ \psi_{2i} &= \tan^{-1}\left[\frac{(L/2+z_i)}{r_m\cos\theta_i}\right] \end{aligned} \tag{2}$$

r_{ij} is the mutual distance between any two ions i and j, and z_i is the coordinate of any ion i and r_m is the adjusted macroion radius (see the appendix).

If, $-L/2 \leqslant z_i \leqslant L/2$, $\theta_i = 0$, otherwise

$$\theta_i = \begin{cases} \sin^{-1}[(z_i - L/2)/r_m], & z_i > L/2 \\ \sin^{-1}[(z_i + L/2)/r_m], & z_i < -L/2. \end{cases} \tag{3}$$

The first term of equation (1) accounts for the Coulombic interaction between the line charge of the spherocylinder and counterions, while the second term is due to mutual interactions between counterions. In the case of a spherocylinder, for a counterion position anywhere on the cylindrical surface ($-L/2 \leqslant z_i \leqslant L/2$), $\theta_i = 0$ and equation (3) does not apply. Then $\psi_{1i} = \tan^{-1}[(L/2-z_i)/r_m]$ and $\psi_{1i} = \tan^{-1}[(L/2+z_i)/r_m]$, and the first term of equation (1) becomes

$$\frac{|e|^2}{4\pi\varepsilon_0\varepsilon_r} C_\lambda Z_c \int_{-\psi_1}^{\psi_2} \sec\varphi \, d\varphi \tag{4}$$

due to the line charge.

If the counterion position is at $|Z_i| \succ L/2$, then $\psi_{2i} = -\theta_i$ and $\psi_{2i} = \tan^{-1}[L/2 + z_i]$ and the first term of equation (1) reduces again to equation (4). For $z_i = (L/2 + R)$, the first term is replaced by $\frac{-|e|^2}{4\pi\varepsilon_0\varepsilon_r} C_\lambda Z_C \ln[\frac{r_m}{r_m+L}]$.

3.1.2. Oblate spheroid ($\tau < 0$).

$$E = \frac{|e|^2}{4\pi\varepsilon_0\varepsilon_r}\left[\sum_i \frac{C_s Z_c}{r_{oi}} + \sum_{i<j}\frac{Z_c^2}{r_{ij}}\right] \tag{5}$$

where $C_s = Z_m$ is the charge at the centre of the oblate spheroid (i.e. at point O in figure 2) and r_{oi} is the distance of a counterion from the centre O. The first term of equation (5) is for the interaction between the charge at the centre O of the oblate spheroid and counterions, and the second term is again due to the mutual interactions between counterions. In this case, $z_i = z_i - L/2$ for $z_i \succ 0$ and $z_i = z_i + L/2$ for $z_i \prec 0$ have been considered to account for the geometry.

3.1.3. Sphere ($\tau = 0$).

$$E = \frac{|e|^2}{4\pi\varepsilon_0\varepsilon_r}\left[\frac{C_s N_c Z_c}{R} + \sum_{i\prec j}\frac{Z_c^2}{r_{ij}}\right] \tag{6}$$

where the first term on the right-hand side is due to the interaction of the macroion charge with the counterions, while the second term accounts for the interaction between the counterions.

It is important to note that the dielectric constant of the macroion is always assumed to be the same as that of counterions. This is a rather common assumption made in the literature to avoid the problem related with electrostatic image due to the discontinuity of the dielectric constant at the interface. However, the effects of a different dielectric constant have been discussed in recent papers by Messina [42].

3.2. Analytical models

3.2.1. WC theory (for spherical macroions). At absolute zero all counterions are physically attached to the macroion surface and thus WC theory can be employed [38, 44] to explain the mechanism. In terms of the WC parameter α [3], the energy gain due to the first overcharging (excess) counterion is

$$\Delta E_1 = \frac{\alpha\lambda Z_c^2}{\sqrt{A}}[(N_c+1)^{3/2} - N_c^{3/2}] + \frac{\lambda Z_c^2}{2R} \tag{7}$$

and similarly, for n excess counterions

$$\Delta E_n = \frac{\alpha\lambda Z_c^2}{\sqrt{A}}[(N_c+n)^{3/2} - N_c^{3/2}] + n^2\frac{\lambda Z_c^2}{2R}. \tag{8}$$

Here, N_c is the total number of counterions necessary to neutralize the macroion, n is the number of overcharging (excess) counterions, $\lambda = \frac{|e|^2}{4\pi\varepsilon_0\varepsilon_r k_B T}$, $\Delta E_1 = E_0 - E_1$ with E_0 being the neutral state energy, and E_1 is the one excess-ion state energy. Also $A = 4\pi a^2$, the macroion surface area, ε_r and ε_0 are the relative and vacuum permittivity respectively, k_B is the Boltzmann constant, Z_c is the counterion valence, and $|e|$ is the charge of a proton. From equation (7) α is given by

$$\alpha = \frac{-(\frac{\lambda Z_c^2}{2R} - \Delta E_1)\sqrt{A}}{\lambda Z_c^2[(N_c+1)^{3/2} - N_c^{3/2}]}. \tag{9}$$

Eliminating α from equation (8), one gets

$$\Delta E_n = -\left(\frac{\lambda Z_c^2}{2R} - \Delta E_1\right)\frac{[(N_c+n)^{3/2} - N_c^{3/2}]}{[(N_c+1)^{3/2} - N_c^{3/2}]} + n^2\frac{\lambda Z_c^2}{2R} \tag{10}$$

where $\Delta E_n = E_0 - E_n$. From equation (10), one can calculate E_n if the first overcharge ΔE_1 is known. The relation [3] for the maximally obtainable number of overcharging counterions is

$$n_{\max} = \frac{9\alpha^2}{32\pi} + \frac{3\alpha}{4\sqrt{\pi}}\sqrt{N_c}\left[1 + \frac{9\alpha^2}{64\pi N_c}\right]^{1/2}. \tag{11}$$

3.2.2. A proposed model modifying the Scatchard approach (for all geometries). A theoretical model to fit the simulation data for all geometries can be proposed by modifying [40] the

Scatchard [41] approach, which employs average interaction. For the macroion complex (with N counterions) of any geometry, the average interaction can be expressed as

$$\langle E_N \rangle = Z_c^2 \langle C \rangle \left[\frac{N(N-1)}{2} \right] - Z_m Z_c \langle M \rangle N \tag{12}$$

$$\langle E_N \rangle = Z_c^2 \langle C \rangle \left[\frac{(N_c+n)(N_c+n-1)}{2} \right] - Z_m Z_c \langle M \rangle (N_c+n) \tag{13}$$

where $N = N_c + n$, $N_c = Z_m/Z_c$ and n is the overcharging counterion. $\langle C \rangle$ and $\langle M \rangle$ represent average counterion–counterion and counterion–macroion energy functions, respectively. $N(N-1)/2$ is the total number of mutual interactions among N counterions on the surface of the macroion. Equation (13) can be expressed in quadratic form in terms of n as

$$\langle E_N \rangle = S_0 + S_1 n + S_2 n^2 \tag{14}$$

where

$$S_0 = Z_c^2 \langle C \rangle \left[\frac{N_c(N_c-1)}{2} \right] - Z_m Z_c \langle M \rangle N_c \tag{15}$$

$$S_1 = \frac{Z_c^2}{2} [2N_c(\langle C \rangle - \langle M \rangle) - \langle C \rangle] \tag{16}$$

$$S_2 = \frac{Z_c^2}{2} \langle C \rangle. \tag{17}$$

The energy difference between a neutral complex and an overcharged one is

$$\begin{aligned} \Delta E_n &= \langle E_N \rangle - \langle E_{N_c} \rangle \\ &= S_1 n + S_2 n^2. \end{aligned} \tag{18}$$

The 'maximal acceptance' n_{max} can be found by differentiating equation (18) with respect to n:

$$\frac{\partial(\Delta E_n)}{\partial n} = S_1 + 2S_2 n + \left(\frac{\partial S_1}{\partial n} \right) n + \left(\frac{\partial S_2}{\partial n} \right) n^2. \tag{19}$$

But

$$\frac{\partial S_i}{\partial n} = \left(\frac{\partial S_i}{\partial \langle C \rangle} \right) \left(\frac{\partial \langle C \rangle}{\partial N} \right) \left(\frac{\partial \langle N \rangle}{\partial n} \right).$$

Since $N = N_c + n$,

$$\frac{\partial S_i}{\partial n} = \left(\frac{\partial S_i}{\partial \langle C \rangle} \right) \left(\frac{\partial \langle C \rangle}{\partial N} \right).$$

Using these identities, equation (19) reduces to

$$\frac{\partial(\Delta E_n)}{\partial n} = S_1 + 2S_2 n + (2N_c - 1) \frac{Z_c^2 n}{2} \left(\frac{\partial \langle C \rangle}{\partial N} \right). \tag{20}$$

For a large number of counterions, one can assume that $\frac{\partial \langle C \rangle}{\partial n} = 0$, since the inclusion of one ion does not make a significant change in the total energy if the counterion number is large enough. This approximation is within the framework of the Scatchard approach. With this approximation, the localization of the minimum in the ΔE_n profile is

$$\begin{aligned} n_{max} &= -\frac{S_1}{2S_2} \\ &= N_c \left[\frac{\langle M \rangle}{\langle C \rangle} - 1 \right] + \frac{1}{2}. \end{aligned} \tag{21}$$

Alternatively,

$$\frac{\langle M\rangle}{\langle C\rangle} = \frac{n_{\max} - 1/2}{N_c} + 1. \tag{22}$$

Using the simulation data, it has been found that $\langle M\rangle/\langle C\rangle$ is approximately constant for a fixed macroion charge, and is almost independent of the macroion geometry. But due to the above-stated approximation the exact value of $\langle M\rangle/\langle C\rangle$ cannot be derived in the above way. To avoid this problem and to get a good fit, a trial and error technique has been employed in the following way.

Like [3], using the first overcharge ΔE_1 from the simulation, $\langle C\rangle$ can be calculated from equation (18) as

$$\langle C\rangle = \frac{\Delta E_1}{Z_c^2\left[1 - \frac{\langle M\rangle}{\langle C\rangle}\right]N_c}. \tag{23}$$

Applying (23) in (18), one can get an expression for the energy as

$$\begin{aligned}\Delta E_n &= \frac{\Delta E_1 n}{2\left[\frac{\langle M\rangle}{\langle C\rangle} - 1\right]N_c}\left\{2\left[\frac{\langle M\rangle}{\langle C\rangle} - 1\right]N_c + 1 - n\right\} \\ &= \frac{\Delta E_1 n}{X N_c}\{X N_c + 1 - n\}\end{aligned} \tag{24}$$

assuming

$$X \cong 2\left[\frac{\langle M\rangle}{\langle C\rangle} - 1\right] \tag{25}$$

as an arbitrary fit parameter.

Using the best values of X obtained by trial and error to fit the simulation data with equation (24), one can calculate $\langle M\rangle/\langle C\rangle$ from equation (25) and can get more accurate $n_{\max}$ by applying it in equation (21).

4. Double macroion auto-ionization

In this case, two macroions 1 and 2 of same size ($\tau_1 = \tau_2$) and of different bare charges Z_1 and Z_2 ($Z_1 \succ Z_2$) surrounded by their neutralizing counterions ($Z_c = 2$) have been considered. The centre–centre separation r between them and the bare macroion charges have been kept fixed. At the beginning of the auto-ionization process, employing the previously stated minimization technique, the number of neutralizing counterions $N_1 = Z_1/Z_c$ and $N_2 = Z_2/Z_c$ are rearranged on the surface of the macroions 1 and 2 respectively to achieve a global minimum energy. Next, a counterion has been chosen randomly from 2 and transferred to 1 and then the energy is minimized again to get the first ionization energy. Practically, this is the same procedure as was followed for the neutral state but the numbers of counterions are now $N_1 + 1$ and $N_2 - 1$ for macroions 1 and 2, respectively. The energies of subsequent ionized states have been calculated by repeating the above procedure.

4.1. Simulation model

4.1.1. A pair of spherocylinders.

$$\begin{aligned}E = \frac{|e|^2}{4\pi\varepsilon_0\varepsilon_r}\Bigg[&C_{\lambda 1} Z_c \sum_i \ln\left[\frac{1+\sin(\psi_{2i})}{1-\sin(\psi_{1i})}\frac{\cos(\psi_{1i})}{\cos(\psi_{2i})}\right] \\ &+ C_{\lambda 2} Z_c \sum_i \ln\left[\frac{1+\sin(\psi_{12i})}{1-\sin(\psi_{11i})}\frac{\cos(\psi_{11i})}{\cos(\psi_{12i})}\right] + \sum_{i<j}\frac{Z_c^2}{r_{ij}}\Bigg]\end{aligned} \tag{26}$$

where

$$C_{\lambda 1} = Z_1/L, \qquad C_{\lambda 2} = Z_2/L, \qquad \psi_{1i} = \tan^{-1}\left[\frac{(L/2 - z_i)}{r_{\mathrm{m}}}\right]$$

$$\text{and} \qquad \psi_{2i} = \tan^{-1}\left[\frac{(L/2 + z_i)}{r_{\mathrm{m}}}\right].$$

If the counterion (figure 7) is at point Q ($Z_i \leqslant L/2$)

$$\psi_{11i} = \sin^{-1}\left[\frac{(L/2 - z_i)}{QT}\right] \qquad \text{and} \qquad \psi_{12i} = \sin^{-1}\left[\frac{(L/2 + z_i)}{QT}\right]$$

or, if the counterion is at point P ($Z_i \succ L/2$)

$$\psi_{11i} = \sin^{-1}\left[\frac{(L/2 - z_i)}{PA}\right] \qquad \text{and} \qquad \psi_{12i} = \sin^{-1}\left[\frac{(L/2 + z_i)}{PB}\right].$$

r_{ij} is the mutual distance between any two ions i and j, irrespective of macroion affiliation, and z_i is the coordinate of any ion i. The distances PA, PB and QT can be calculated from the ion coordinates. Although in figure 7 points P and Q are on macroion 1, they could be on either macroion without any change in above-stated principle.

4.1.2. A pair of oblate spheroids.

$$E = \frac{|e|^2}{4\pi\varepsilon_0\varepsilon_{\mathrm{r}}}\left[\sum_i \frac{C_{s1}Z_{\mathrm{c}}}{r_{oi}} + \sum_i \frac{C_{s2}Z_{\mathrm{c}}}{r_{oi}} + \sum_{i<j} \frac{Z_{\mathrm{c}}^2}{r_{ij}}\right] \tag{27}$$

where$C_{s1} = Z_1$ and $C_{s2} = Z_2$.

4.1.3. A pair of spheres.

$$E = \frac{|e|^2}{4\pi\varepsilon_0\varepsilon_{\mathrm{r}}}\left[\frac{C_{s1}N_{\mathrm{c}}Z_{\mathrm{c}}}{R} + \frac{C_{s2}N_{\mathrm{c}}Z_{\mathrm{c}}}{R} + \sum_{i<j} \frac{Z_{\mathrm{c}}^2}{r_{ij}}\right]. \tag{28}$$

All other notations and symbols are the same as those of the single macroion case.

4.2. Analytical models

4.2.1. WC theory (for spherical macroions). Since the total electrostatic potential energy is comprised of overcharging and undercharging of macroions, one can write the energy gain due to ionization as [3]

$$\Delta E_n^{\mathrm{ion}} = \Delta E_n^{\mathrm{ovr}} + \Delta E_n^{\mathrm{und}} \tag{29}$$

where n is the degree of ionization. The energy gain due to overcharging and undercharging can be written analogously to equation (8) as

$$\Delta E_n^{\mathrm{ovr}} = \frac{\alpha\lambda Z_{\mathrm{c}}^2}{\sqrt{A}}\left[(N_1 + n)^{3/2} - N_1^{3/2}\right] + n^2\frac{\lambda Z_{\mathrm{c}}^2}{2R} \tag{30}$$

$$\Delta E_n^{\mathrm{und}} = \frac{\alpha\lambda Z_{\mathrm{c}}^2}{\sqrt{A}}\left[(N_2 - n)^{3/2} - N_2^{3/2}\right] + n^2\frac{\lambda Z_{\mathrm{c}}^2}{2R}. \tag{31}$$

4.2.2. Modified Scatchard model. As before, the average energies of macroions 1 and 2 can be expressed as

$$\langle E_1\rangle = Z_c^2\left[\frac{N_1(N_1-1)}{2}\right]C_1 - Z_1Z_c\langle M_1\rangle - Z_2Z_c\langle M\rangle \tag{32}$$

$$\langle E_2\rangle = Z_c^2\left[\frac{N_2(N_2-1)}{2}\right]C_2 - Z_2Z_c\langle M_2\rangle - Z_1Z_c\langle M\rangle \tag{33}$$

where, like the single macroion case, C_1, C_2, M_1, M_2 are the average energy functions between counterion–counterion and counterion–macroion for macroions 1 and 2 and M is the counterion–macroion average energy function between macroion 2 and a counterion on macroion1 (or macroion 1 and a counterion on macroion 2). Since, in this case, the sizes of both macroions are equal, $M_1 = M_2$. For n degrees of ionization $N_1 = N_1 + n$ and $N_2 = N_2 - n$, and the total average energy of the pair is

$$\langle E_n\rangle = \langle E_1\rangle + \langle E_2\rangle. \tag{34}$$

The energy gain due to n degrees of ionization is

$$\langle \Delta E_n^{\text{ion}}\rangle = \langle E_n\rangle - \langle E_0\rangle \tag{35}$$

where $\langle E_0\rangle$ is the energy of the neutral state ($n = 0$). Applying equations (32) and (33), equation (35) reduces to

$$\langle \Delta E_n^{\text{ion}}\rangle = Z_c^2\left[n^2\frac{C_1+C_2}{2} + n\left\{\frac{C_2}{2} - \frac{C_1}{2} + f(C_1, M_1, M)\right\}\right]. \tag{36}$$

Using the simulation value of first ionization in equation (26), the last term of equation (26) can be calculated as

$$f(C_1, M_1, M) = \frac{\langle \Delta E_1\rangle}{Z_c^2} - C_2. \tag{37}$$

From equations (36) and (37)

$$\langle \Delta E_n^{\text{ion}}\rangle = Z_c^2\left[n^2\frac{C_1+C_2}{2} + n\left\{\frac{\langle \Delta E_1\rangle}{Z_c^2} - \frac{C_1+C_2}{2}\right\}\right]. \tag{38}$$

Considering $X = \frac{C_1+C_2}{2}$ as a fit parameter, one can rewrite equation (38) as

$$\langle \Delta E_n^{\text{ion}}\rangle = Z_c^2\left[n^2X + n\left\{\frac{\langle \Delta E_1\rangle}{Z_c^2} - X\right\}\right]. \tag{39}$$

5. Results and discussion

To conform with the previous work of Messina *et al* [3] the same parameters have been considered for all cases, as given in table 1 (see also table 1 of [3]) to facilitate the comparison of the present results with those of [3]. The macroion and counterion sizes have been chosen such as to minimize the excluded volume effect. Electrostatic interaction energies have been calculated in dimensionless forms by normalizing to the standard thermal energy $k_BT = 4.1124 \times 10^{-21}$ J/particle.

5.1. Single macroion case

The ground state configuration energy of a spherical macroion versus the number of overcharging counterions has been plotted in figure 4. For lower macroion charge [$Z_m = 50$], the energy variation is almost the same as those given in figure 5 of [3]. With the increase

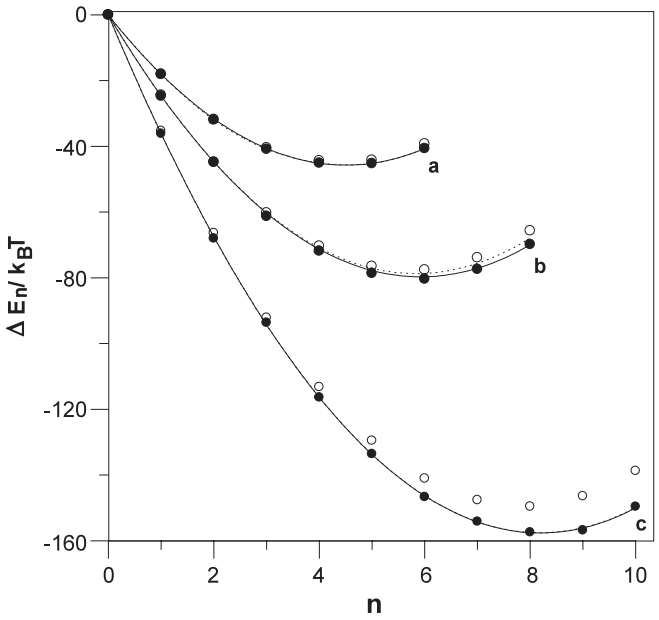

Figure 4. The ground state electrostatic energy of a charged spherical macroion as a function of overcharging counterions. Open circles are from [3] and [43], filled circles are from this work and the dashed and solid lines are from equations (10) and (24), respectively. The neutral state energies of a spherical macroion of corresponding charges have been taken as the origin of the plot. Curves a, b and c are for $Z_m = 50$, 90 and 180, respectively.

Table 1. Physical parameters and symbols used in the present calculations.

Room temperature $T = 298$ K
Relative permittivity $\varepsilon_r = 16.0$
Valence of counterion $Z_c = 2$
Valence of macroion ion $Z_m = 50, 90, 180$
Lennard-Jones length unit $\sigma = 3.57$ Å
Counterion diameter $= \sigma$
Radius of a spherical macroion $= R$
Radius of a non spherical macroion $= r_m$
Macroion (spherical)–counterion distance of closest approach $= 8\sigma \cong 28.56$ Å

of macroion charge the results clearly show a gradual deviation from the corresponding result in Messina *et al* [3]. This should not be too surprising since Messina *et al* used different colloid–counterion potentials. For instance, in their work the excluded volume interactions were considered via the repulsive part of the Lennard-Jones (LJ) potential where counterions could penetrate up to 0.5σ inside the *soft* macroion. Both the Coulombic and excluded volume interactions contributed to the total potential in the MD simulation. Within the framework of the present technique, it is seen that the addition of the repulsive component of the LJ potential cannot decrease the total interaction energy of the configurations due to the nature of the potential. Thus, counterion penetration into the macroion is automatically rejected by this technique as though the macroion and counterions were hard spheres. In the case of smaller systems (namely, $Z_m = 50$) the counterions hardly encounter each other or penetrate into the macroion due to comparatively weaker Coulombic interaction, and thus the results of the

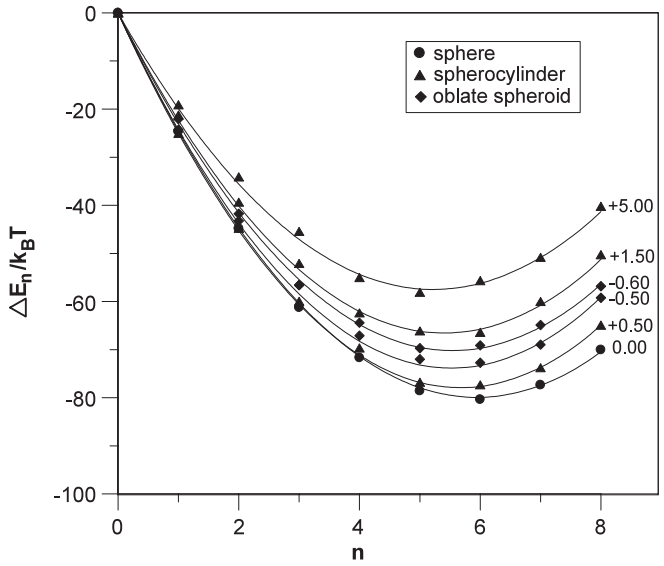

Figure 5. The ground state electrostatic energy of charged ($Z_m = 90$) macroions of different τ (namely, sphere ($\tau = 0$), oblate spheroid ($\tau \prec 0$) and spherocylinder ($\tau \succ 0$)) as a function of overcharging counterions n. The neutral state energy of each size and geometry (indicated by τ) is the origin of the corresponding curves. For both the non-spherical geometries the lowest energy points (energy corresponds to 'maximal acceptance' n_{max}) shift upwards with the increase of $|\tau|$. The solid lines are theoretical fits from equation (24). The fit parameters are given in table 4.

present study for smaller systems are very close to those from MD calculations. In larger systems (namely, $N_c = 45, 90$) however, the LJ potential in the MD calculation plays an important role in ion distribution due to shorter distances ($\leqslant 2^{1/6}\sigma$) between the counterions and to their being able to penetrate inside the macroion. Obviously, for higher numbers of counterions, the two techniques (MD and the present) actually consider different physical conditions, and thus it is not worthwhile to attribute superiority to either of them.

From the first overcharge, as explained earlier, α has been calculated from equation (9). Using this α in equation (8), a curve (dashed curves of figure 4) has been found that fits well with all the data resulting from this technique. This comparison clearly reveals the computational accuracy and reliability of this method. The solid curves are from equation (24). The agreement between the two models is obviously excellent.

The line charge distribution for a spherocylinder is a very common representation for cylindrical macroions. Under this assumption it is found that when the non-spherical macroions are gradually overcharged, the potential energy varies very similarly to that of a spherical macroion. In figure 5, the similarity between the potential energy curves of non-spherical macroions and those of a spherical one is obvious, with a minimum ('maximal acceptance') for all the three geometries (macroion charge $Z_m = 90$). Studies on other non-spherical macroion charges have shown similar results. Each curve is labelled by the corresponding factor τ with $\tau = 0$, $\tau > 0$ and $\tau < 0$ indicating sphere, spherocylinder and oblate spheroid, respectively. The solid curves have been produced using equation (24). The fit parameters for equation (24) are given in table 4. The excellent agreement indicates that the proposed theoretical model (derived by modifying the Scatchard approach) is equally suitable for all three geometries.

In both the non-spherical cases, the minima of the interaction energy shift upwards (become more positive) with the increase of $|\tau|$. From figures 2 and 3, it is obvious that an increase

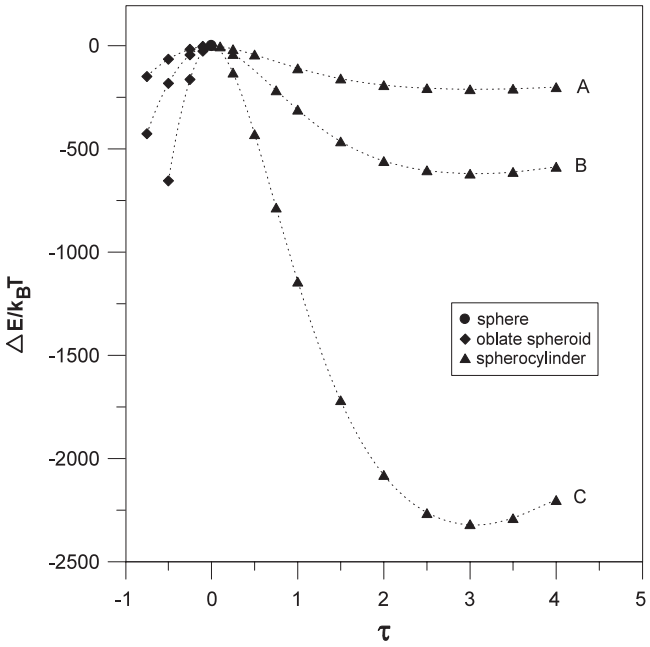

Figure 6. The neutral state energy of macroions with different bare charges: (A) $Z_m = 50$, (B) $Z_m = 90$ and (C) $Z_m = 180$ as a function of τ. The neutral state energy of a sphere is taken as the origin. The dashed lines are polynomial fits to guide the eye.

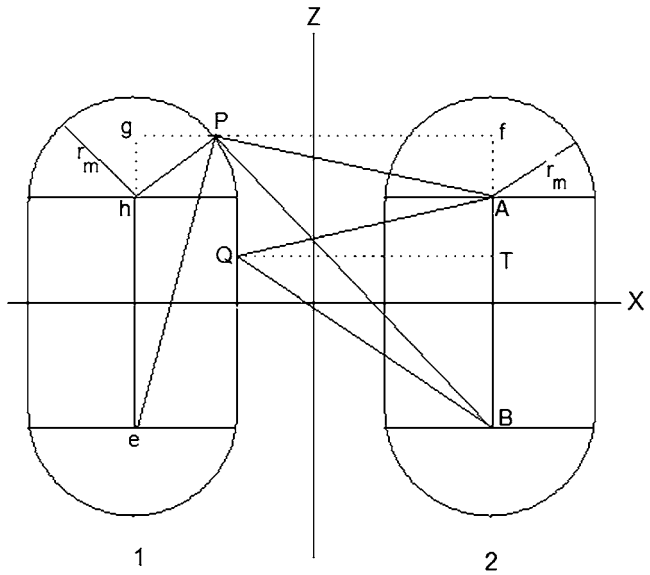

Figure 7. A spherocylindrical macroion pair, where $\psi_1 = \angle$gPh, $\psi_2 = \angle$gPe, $\psi_{11} = \angle$fPA, $\psi_{12} = \angle$fPB for a counterion at P on macroion 1. For any position of any counterion on any macroion can be specified in the similar way.

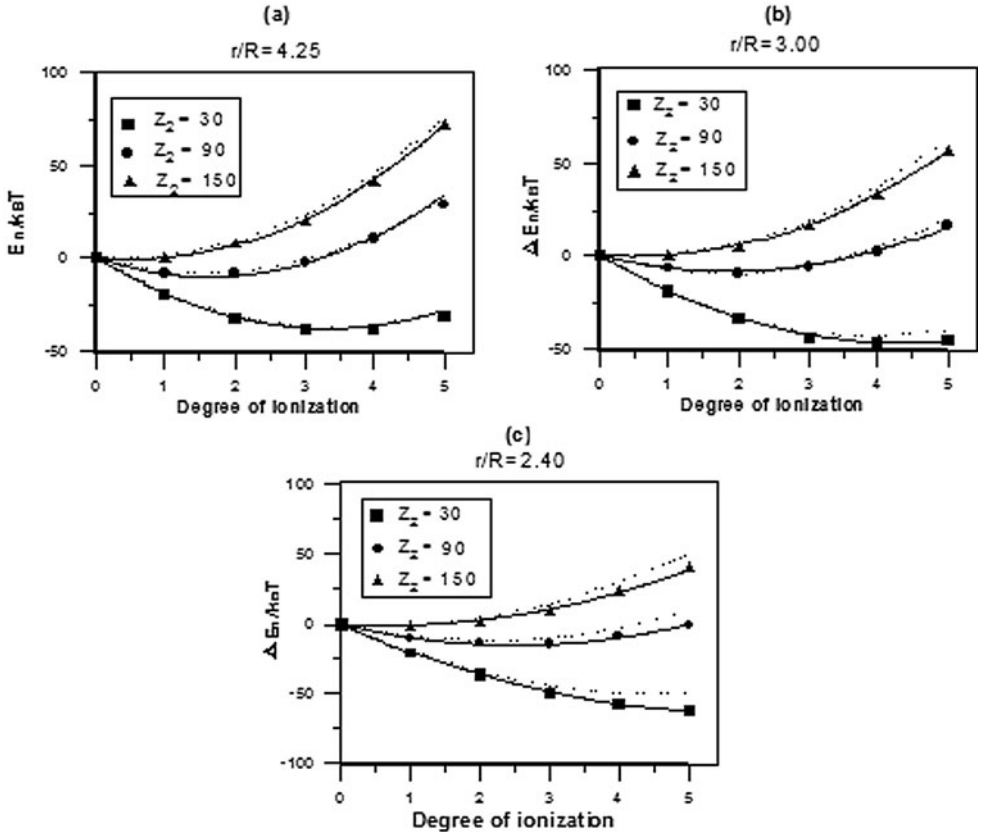

Figure 8. The total electrostatic potential energy of a pair of spherical macroions as a function of the degree of ionization. The charge Z_1 of macroion 1 is always fixed at 180 while the charge Z_2 of other one varies as shown. The neutral state energy has been considered as the origin. The centre–centre macroion separations are (a) $r/R = 4.25$ (b) $r/R = 3.0$ and (c) $r/R = 2.4$. The dashed and solid curves are from equations (29) (WC theory) and (39) (proposed model), respectively. Some of the fit parameters of equation (39) are given in table 5.

of $|\tau|$ for an oblate spheroid means a decrease of its thickness, while for a spherocylinder an increase of $|\tau|$ implies an increase of its length. Since in both geometries the surfaces are kept always the same as that of a sphere of radius R (=28.56 Å), the increase of $|\tau|$ makes them narrower, bringing the surfaces closer to the line charge for a spherocylinder and to the central point charge for an oblate spheroid. Due to this, the interaction energy should decrease (become more negative), but we see the opposite in figure 5. This can be explained in the following way. In an oblate spheroid, with the increase of $|\tau|$ the counterions come closer to one another, causing increased repulsion among them. The repulsive part of the total interaction energy becomes more significant than the attractive one. In a spherocylinder, an increase of the surface area (on the cylindrical region of the macroion) decreases the repulsion among the counterions. At the same time, the line charge density also decreases, which causes a decrease in attraction between the line charge and the counterions. Due to this competitive decrease of attractive and repulsive interaction energies, the increase in total energy with $|\tau|$ is much slower for a spherocylinder than that for an oblate spheroid.

With the increase of $|\tau|$, the surface of the oblate spheroid comes closer to the point O (figure 3) where the macroion charge is assumed to be concentrated, and this causes a very

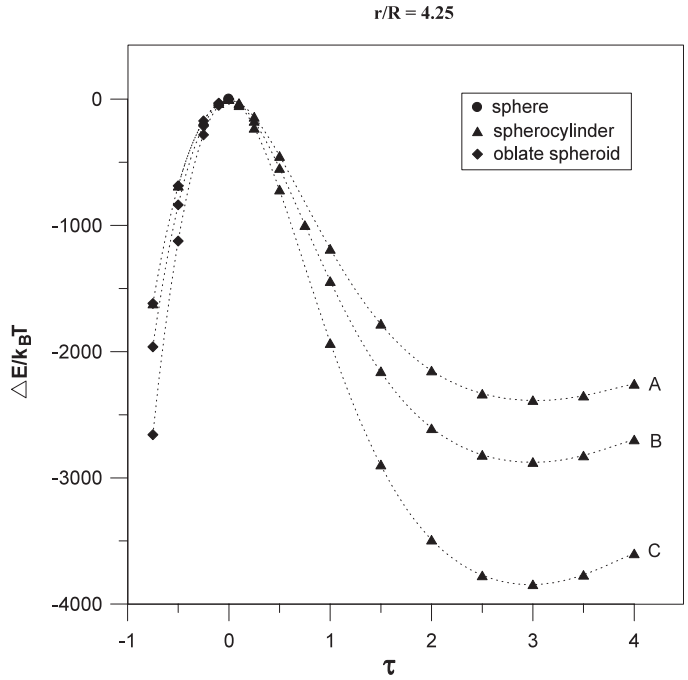

Figure 9. The neutral state energy of a pair of macroions separated by a centre–centre distance $r = 121.38$ Å ($r/R = 4.25$) as a function of τ. The charge of one macroion is fixed at $Z_1 = 180$ while that of the other varies as: (A) $Z_m = 30$, (B) $Z_m = 90$ and (C) $Z_m = 150$. The dashed lines are merely to guide the eyes.

strong attractive interaction between the counterions and macroion. By the same token, the area where the counterions find themselves shrinks, and repulsion among them also becomes high. In such a situation any excess counterion, due to overcharging, would further enhance both such attraction and repulsion. Such competing effects are likely to cause a fluctuation in total energy. This fluctuation has seen to occur at $\tau \leqslant -0.75$, and thus curves with $\tau \leqslant -0.75$ are not shown in figure 5.

Figure 6 shows that due to an increase of $|\tau|$ the neutral state energy of both geometries decreases, but the decrease is much more rapid for an oblate spheroid than for a spherocylinder due to the reason explained above. The most significant feature of figure 6 is that the neutral state energy of the spherocylinder also has minima at some length of the cylinder similar to the overcharging curves in figure 4.

It is obvious from figure 6 that the energy of the neutral state is a continuous function of τ which shows the dependence of Coulombic interaction energy with shape and size of a charged particle. In WC theory, the energy is inversely proportional to the square root of the surface area of the macroion. The surface of an oblate spheroid or a spherocylinder is actually a function of τ. This is why the macroion–counterion interaction energy is also a function of τ. In non-neutral cases (such as maximally overcharged states) we also found curves similar to figure 6.

5.2. Double macroion case

In this case, for all geometries, the sizes of both the macroions of a pair of any geometry are the same. Also, like the single macroion case, the surface areas of the macroions are the same for all geometries.

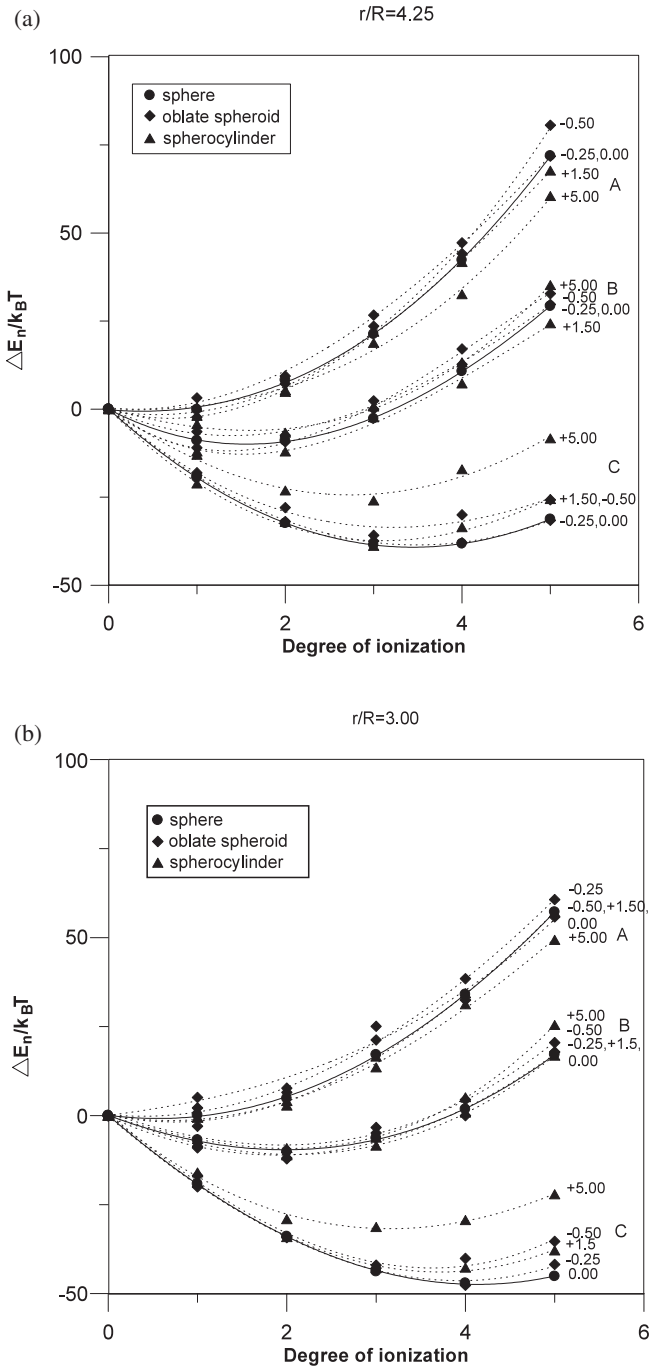

Figure 10. The total electrostatic potential energies of pairs of macroions with different geometries as a function of the degree of ionization (similar to figure 8). (A) $Z_2 = 150$, (B) $Z_2 = 90$ and (C) $Z_2 = 30$. The centre–centre distances are: (a) $r/R = 4.25$, (b) $r/R = 3.00$ and (c) $r/R = 2.40$ as shown in figures (a)–(c) respectively. The dashed and solid lines are polynomial fits to guide the eyes. Solid curves represent spherical macroions.

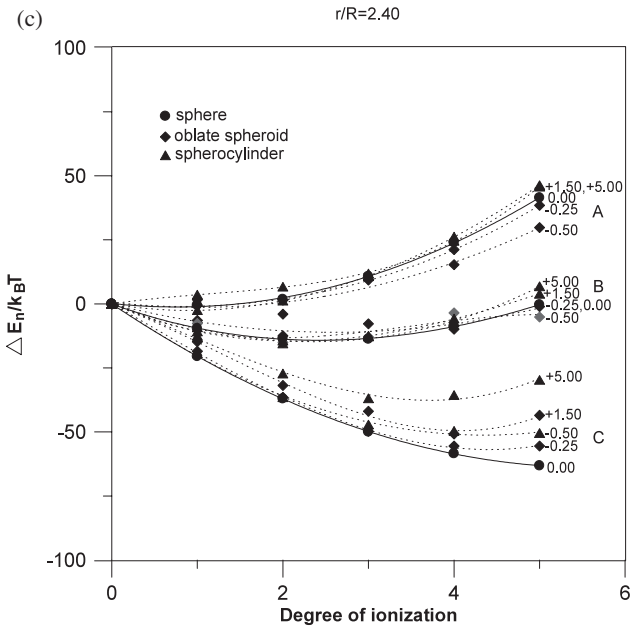

Figure 10. (Continued.)

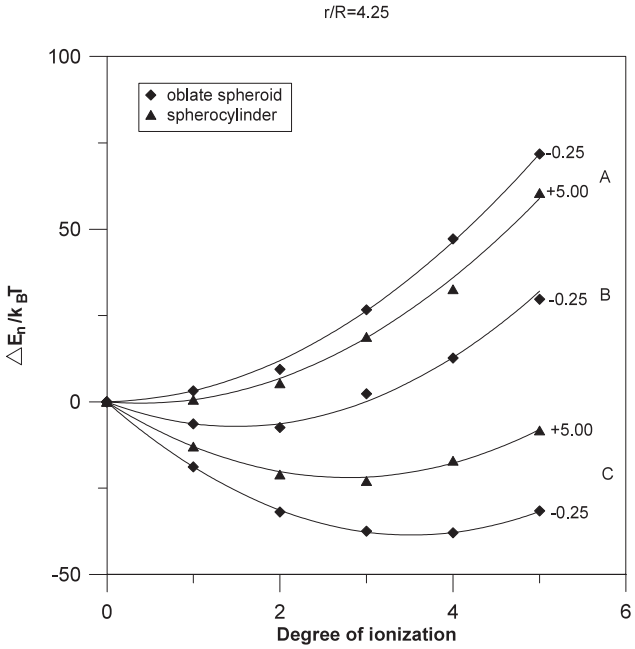

Figure 11. A comparison between the proposed theoretical model (solid curves) and the simulation. The solid curves are from equation (39). The fit parameters are given in table 5.

Figure 8 is a comparison between simulation results and theoretical predictions for spherical double macroions. The solid lines are from equation (39). Some of the fit parameters of equation (39) is given in table 5 ($\tau = 0.0$). The excellent agreement clearly indicates

Table 2. A comparison between the ground state electrostatic energies calculated from present technique (column 3) and WC theory (equation (8)) for three different values of α (column 4–6) and from MD (column 7).

			WC			
Z_m	n	Simulation	$\alpha = 1.956$	$\alpha = 1.920$	$\alpha = 1.960$	Reference [3, 43]
	0	0	0	0	0	0
	1	−18.060	−18.060	−17.683	−18.102	−17.988
	2	−31.955	−31.611	−30.848	−31.695	−31.747
	3	−40.843	−40.644	−39.489	−40.772	−40.423
50	4	−45.051	−45.152	−43.598	−45.324	−44.348
	5	−45.192	−45.129	−43.169	−45.346	−44.159
	6	−40.651	−40.569	−38.195	−40.832	−39.206
			$\alpha = 1.935$	$\alpha = 1.880$	$\alpha = 1.960$	
	0	0	0	0	0	0
	1	−24.596	−24.596	−23.884	−25.005	−24.379
	2	−44.747	−44.578	−43.148	−45.402	−44.220
	3	−61.233	−54.945	−57.788	−61.187	−60.237
90	4	−71.814	−70.693	−67.801	−72.357	−70.302
	5	−78.566	−76.814	−73.185	−78.910	−76.464
	6	−80.346	−78.320	−73.937	−80.843	−77.567
	7	−77.389	−75.193	−70.053	−78.152	−73.859
	8	−69.998	−67.436	−61.532	−70.834	−65.639
			$\alpha = 1.930$	$\alpha = 1.880$	$\alpha = 1.960$	
	0	0	0	0	0	0
	1	−36.132	−36.132	−34.692	−36.272	−35.270
	2	−67.980	−67.569	−64.679	−67.850	−66.340
	3	−93.616	−94.308	−89.962	−94.731	−92.110
180	4	−116.330	−116.349	−110.540	−116.914	−113.160
	5	−133.502	−133.699	−126.409	−134.399	−129.480
	6	−146.658	−146.333	−137.571	−147.185	−141.040
	7	−154.154	−154.271	−144.024	−155.270	−147.580
	8	−157.432	−157.511	−145.766	−158.653	−149.560
	9	−156.793	−156.045	−142.798	−157.333	−146.380
	10	−149.601	−149.875	−135.117	151.310	−138.710

that the proposed model (equation (39)) can explain the simulation better than WC theory (equation (29)). The simulation results look very much like those of MD [3]. Unlike single macroion overcharging (figure 4), the published results using the LJ potential in an MD simulation [3] do not seem to be very different from those of this technique obtained using a hard sphere potential. Nevertheless, it can be expected that the energy calculated from the present technique should be a little lower than those yielded by an MD simulation, due to the same reason stated in the case of a single macroion. Note that the only purpose of this part of the study (figure 8) is to check the validity of the present technique, and thus the discussion of this figure (already given in [3]) has been omitted here.

Figure 9 shows the neutral ground state energy variation with τ for a double macroion at a fixed macroion separation where the charge of one macroion is fixed to $Z_1 = 180$ while the charge Z_2 of the other one varies. As expected, the energy gain increases with the magnitude of the charge Z_2. The similarities in shapes of the curves between the two cases (single (figure 6) and double macroion) are notable. All the properties, namely minima at a certain length of

Table 3. Comparison between the WC parameter α obtained from table 2 of [3] and those from calculations using the present technique (equation (9)).

Z_m	N_c	α (this work)	α [3]
4	2	1.894	1.890
6	3	1.884	1.970
8	4	1.894	1.920
10	5	2.005	2.020
20	10	1.911	1.930
30	15	1.954	1.910
32	16	1.956	
50	25	1.956	1.920
90	45	1.935	1.880
128	64	1.956	
150	75	1.990	1.910
180	90	1.930	1.88
288	144	1.867	
360	180	1.835	1.860

Table 4. Proposed theoretical model (equation (24)) fit parameters (X) for the single macroion case (figures 4 and 5).

τ	X	τ	X
+5.00	0.210	0.00	0.242
+1.50	0.218	−0.50	0.223
+0.50	0.230	−0.60	0.224

Table 5. Proposed theoretical model (equation (39)) fit parameters (X) for the double macroion case (figures 8 and 11). The centre–centre separation is 121.38 Å ($r/R = 4.25$).

τ	$Z_2 = 150$	$Z_2 = 90$	$Z_2 = 30$
+5.00	0.700		0.710
0.00	0.905	0.925	0.825
−0.25	0.700	0.800	0.780

the spherocylinder, continuous variation of energy with τ, etc, of the single macroion case are also present in the case of a double macroion.

Figure 10 shows a comparison of the energy gain corresponding to the 'degree of ionization' (DI) between macroions of three different geometries. The calculations have been done in exactly the same way and with the same macroion charges and centre to centre separations as the spherical cases (figure 8). The energy gains for non-spherical macroions at each DI and centre to centre distance are very similar to those of the spherical cases except for higher macroion charge separation ($Z_2 = 30$). This indicates that the ionic correlation between the condensed ions is almost independent of macroion geometry and size if the charge asymmetry is not too high. Consequently, the long range Coulomb interaction between a pair of macroions with low charge separation can be expected to be independent of their size and geometry.

Figure 11 shows a verification of the proposed theoretical model by simulation data using some of the results of figure 10(A) (for clarity, other curves are not shown). The fit parameters can be found in table 5. Again, the excellent agreement clearly shows that the model is suitable for all geometries.

Table 2 summarizes the numerical results for direct comparison with the corresponding numerical values from the work of Messina *et al* [3, 43]. Columns 3, 4 and 7 have already been

shown graphically in figure 4, where the dots are column 3, dashed lines are column 4 and the open circles are column 7. Using the first overcharge ΔE_1 (simulation) from column 3, the WC parameter α has been calculated from equation (9). Applying those α in equation (8), column 4 has been calculated. The close proximity between the values in the two columns 3 and 4 clearly reveals excellent agreement between this technique and the WC theory. Columns 5 and 6 have been calculated using α given in [3] and WC planar α (=1.96) respectively from equation (8). Since in all three cases ($Z_m = 50, 90, 180$) the α of the present results are very close to planar α, the results are also very similar (see columns 3 and 6). Column 7 is the MD simulation result published in [3]. All the results in table 2 are in good numerical agreement overall, justifying the validity and accuracy of the present technique.

In table 3, values of α have been calculated for various cases and compared with those given in [3]. Again, good agreement between the two sets of α calculated using the two different techniques is obvious.

6. Concluding remarks

In this paper, the phenomenon of overcharging of macroions with different geometries and sizes has been studied using a simple technique based on electrostatic Coulombic interaction energy minimization. The performance of the technique has been verified in a published MD study [3] for spherical macroion cases. It is found that the technique is straightforward to use, economic in terms of computer time usage, and equally efficient to study the overcharging phenomenon for both single and double macroion cases including different macroion geometries and sizes.

Note that the technique is comprised of three different steps, and the second step has some similarities with traditional MC simulation, namely random movement of ions. Usually, in almost all types of MC methods (Markov chain MC or sequential MC), the random sampling is governed by a defined probability (e.g. Boltzmann distribution for Markov chain MC) distribution function. In this technique the probability of acceptance of a move is either 1 or 0. Traditional MC simulation, for example standard Metropolis MC, generates a number of equally likely configurations (after equilibration) and then takes an average over all those configurations to produce the final result. However, in this technique there is no need to equilibrate the system; all accepted configurations are considered. Any accepted configuration must have lower energy than previous one. But in Metropolis MC, higher energy configurations can also be accepted on a random basis (uphill). This is why the final configuration produced by this technique has the lowest potential energy.

The most significant feature of this technique is the introduction of the concept of a randomly varying displacement parameter (DP), which helps the system reach very close to its true ground state, while in Metropolis MC simulation the DP is fixed to a value that generally yields 50% acceptance of the random move. This is why the traditional Metropolis MC is not useful for studying the overcharging phenomenon where the breaking of recurrent special counterion arrangements resulting in metastable local minima is required.

On the other hand, the basic difference of the present technique from simulated annealing proposed by Kirkpatric *et al* [45] (which is a Metropolis MC algorithm) is that there is no need to consider adiabatic cooling to reach the frozen state for this technique, as it always deals with absolute zero from the very beginning. As in an MD simulation, the system does not need to be heated up periodically to overcome potential energy barriers, since in the present technique those energy barriers are being surmounted by automatic adjustment (sudden increase at local minima) of the DP. Although both an increase of the system temperature and enhancement of the DP have similar effects on ionic movements, the degrees of freedom are fewer in the latter case as the ions are confined to move only over the macroion surface, resulting in less

computer time being needed than in the previous case. Moreover, there is no cell surrounding the macroion in the present technique since the counterions are restricted to move over the surface of the macroion.

The other possible way to overcome the energy barriers is embedded in the intrinsic nature of the technique itself. To move an ion, this technique does not consider any energy barrier or energy pitfall in between any two consecutive positions of the ion. A randomly selected ion at any initial position can simply vanish and can evolve in another position if and only if this movement can cause a decrease in the total system energy. In this case the DP may not be increased to cross a barrier which has also been observed in some situations. From these two possible ways of surmounting energy barriers it can be assumed that if the width of the barrier is bigger than the current DP, only then will the DP adjust itself to allow a bigger movement of the ion so that it can evolve to a lower energy state (if there is any) across the barrier.

All data points are seen to be well fitted with the equations (10) and (29) (for spherical geometry) based on a simple version of WC theory [3] and also with equations (24) and (39) (for all geometries) derived by modifying the Scatchard approach.

In the case of a double macroion, this technique clearly indicates that at absolute zero stable ionized states can exist as they are energetically favourable, and those states are influenced by macroion geometry at higher charge asymmetry. In future studies, a traditional MC simulation, such as Metropolis MC, will be used to check whether these ionized states exist at room temperature and in solution with salt.

Acknowledgments

AKM expresses gratitude to Professor K S Schmitz, Professor L B Bhuiyan and Professor L Fonseca for valuable discussions on some aspects of this work and to R Messina and C Holm for providing data and e-mail correspondence.

Appendix

The radius of the cylinder and the end caps of the spherocylinder are equal. With the change of the length of the cylinder, this radius has to change to keep the surface area the same as that of a sphere of radius R. This has been done in the following way.

$$4\pi r_{\mathrm{m}}^2 + 2\pi r_{\mathrm{m}} L = 4\pi R^2 \tag{A.1}$$

where r_{m} is the new adjusted radius and L is the length of the cylinder. With $L = r_{\mathrm{m}}\tau$, equation (A.1) reduces to

$$r_{\mathrm{m}} = \frac{R}{\left[\frac{1}{2}\tau + 1\right]^{1/2}}, \qquad \tau \succ 0. \tag{A.2}$$

Similarly, in the case of an oblate spheroid,

$$r_{\mathrm{m}} = \frac{R}{\left[\frac{1}{2}\tau + 1\right]^{1/2}}, \qquad \tau \prec 0. \tag{A.3}$$

References

[1] Butler J C, Angelini T, Tang J X and Wong G C L 2003 *Phys. Rev. Lett.* **91** 028301
[2] Golestanian R and Liverpool T B 2002 *Phys. Rev.* E **66** 051802
[3] Messina R, Holm C and Kremer K 2001 *Phys. Rev.* E **64** 021405

[4] Messina R, Holm C and Kremer K 2001 *Phys. Rev. Lett.* **85** 872
[5] Messina R, Holm C and Kremer K 2001 *Eur. Phys.* **4** 363
[6] Nguyen T T, Grosberg A and Shklovskii B I 2000 *J. Chem. Phys.* **113** 1110
[7] Greberg H and Kjellander R 1998 *J. Chem. Phys.* **108** 2940
Gonzales-Tovar E, Lozada-Cassou M and Henderson D 1985 *J. Chem. Phys.* **83** 361
[8] Shklovskii B I 1999 *Phys. Rev.* E **60** 5802
[9] Perel V I and Shklovskii B I 1999 *Physica* A **274** 446
[10] Nguyen T T and Shklovskii B I 2001 *Phys. Rev.* E **64** 041407
Guldbrand L, Jönsson B, Wennerström H and Linse P 1984 *J. Chem. Phys.* **80** 2221
[11] Podgornik R, Akesson T and Jönsson B 1995 *J. Chem. Phys.* **102** 9423
[12] Neu J C 1999 *Phys. Rev. Lett.* **82** 1072
[13] Sader J E and Chan D Y C 1999 *J. Colloid Interface Sci.* **213** 268
[14] Trizac E and Raimbault J L 1999 *Phys. Rev.* E **60** 6530
[15] Verwey E J W and Overbeek J Th G 1948 *Theory of the Stability of Lyophobic Colloids* (Amsterdam: Elsevier)
[16] Thomson J J 1904 *Phil. Mag.* **7** 237
[17] White L L 1952 *Am. Math. Mon.* **59** 606
[18] Marx E 1970 *J. Franklin Inst.* **290** 71
[19] Melnyk T W, Knop O and Smith W R 1977 *Can. J. Chem.* **55** 1745
[20] Wille L T 1984 *Nature* **324** 46
[21] Berezin A A 1985 *Am. J. Phys.* **53** 1037
[22] Ashby N and Brittin W E 1986 *Am. J. Phys.* **54** 776
[23] Calkin M G, Kiang D and Tindall D A 1986 *Nature* **319** 454
[24] Aspden H 1987 *Am. J. Phys.* **55** 199
[25] Weinrach J B, Carter K L, Bennett D W and McDowell H K 1990 *J. Chem. Educ.* **67** 995
[26] Erber T and Hockney G M 1991 *J. Phys. A: Math. Gen.* **24** L1369
[27] Glasser L and Every A G 1992 *J. Phys. A: Math. Gen.* **25** 2473
[28] Edmundson J R 1992 *Acta Crystallogr.* A **48** 60
[29] Edmundson J R 1993 *Acta Crystallogr.* A **49** 648
[30] Altschuler E L, Williams T J, Ratner E R, Dowla F and Wooten F 1994 *Phys. Rev. Lett.* **72** 2671
[31] Altschuler E L, Williams T J, Ratner E R, Dowla F and Wooten F 1995 *Phys. Rev. Lett.* **74** 1483
[32] Erber T and Hockney G M 1995 *Phys. Rev. Lett.* **74** 1482
[33] Pérez-Garrido A, Ortuño M, Cuevas E and Ruiz J 1996 *J. Phys. A: Math. Gen.* **29** 1973
[34] Morris J R, Deaven D M and Ho K M 1996 *Phys. Rev.* B **53** R1740
[35] Kuiljaars A B J and Saff E B 1997 *Math. Intell.* **19** 5
[36] Pérez-Garrido A and Moore M A 1999 *Phys. Rev.* B **60** 15628
[37] Bowick M, Cacciuto A, Nelson D R and Travesset A 2002 *Phys. Rev. Lett.* **89** 185502 (*Preprint* cond-matt/0206144)
[38] Levin Y and Arenzon J J 2003 *Europhys. Lett.* **63** 415
[39] Patra M, Patriarca M and Karttunen M 2003 *Phys. Rev.* E **67** 031402
[40] Schmitz K S 1999 *Langmuir* **15** 2854
[41] Scatchard G 1949 *Ann. New York Acad. Sci.* **51** 660
[42] Messina R 2002 *Preprint* cond-mat/0204550
[43] Messina R and Holm C 2001 personal communication
[44] Shklovskii B I 1999 *Phys. Rev. Lett.* **82** 3268
[45] Kirkpatric S, Gelatt C D and Vecchi M P 1963 *Science* **220** 671